EARTHQUAKE ENGINEERING AND STRUCTURAL DYNAMICS
Earthquake Engng. Struct. Dyn. **28**, 1651–1667 (1999)

TWO-DIMENSIONAL SCATTERING OF IN-PLANE BODY WAVES DUE TO A DISCONTINUITY IN BEDROCK

ERNEST HEYMSFIELD*
Department of Civil and Environmental Engineering, Louisiana State University, 3508 CEBA Building, Baton Rouge, LA 70803, USA

SUMMARY

The direct boundary integral equation technique is used to study in-plane surface amplification of in-plane seismic body waves for the case of an inhomogeneity in a bedrock half-space. In the studied soil configuration, a soil layer rests on a rock half-space which includes a rock inclusion. The rock inclusion considered is a semi-infinite horizontal rock layer in which its upper boundary borders the soil layer. Materials in the soil–rock configuration are considered viscoelastic except for the section of the rock half-space below the level of the rock inclusion which is considered elastic. A parametric study is performed to determine controlling factors for surface displacement due to in-plane body waves. The study investigates varying the stiffness and the thickness of the rock inclusion for a range of frequencies and wave incidence angles. Anti-plane waves for this type of soil-rock configuration have been addressed in a previous article by Heymsfield (*Earthquake Engng. Struct. Dyn.* **28**: 841–855 (1999)).

KEY WORDS: soil amplification; seismic waves; rock discontinuity; boundary elements

INTRODUCTION

As seismic waves propagate through the earth's near surface geology, earthquake motion can be greatly modified causing significant variation of the seismic motion along the surface.[2] Historical records of regional surface displacements testify to this phenomena. Two recent examples of this variability of surface amplification are the Mexico City Valley included in an article by Rial *et al.*[3] and the Northridge earthquake in an article by Finn *et al.*[4] In these studies, the variance of the surface displacement can be correlated to the soil geology.

Exact solutions for the amplification of in-plane seismic waves are limited to the one-dimensional solution. In this solution, seismic motion is assumed to propagate through horizontal layers of homogeneous and isotropic material. Although the one-dimensional solution is commonly used, a deficiency in the method is that it neglects the effect of any anomaly, whether in

* Correspondence to: Ernest Heymsfield, Department of Civil and Environmental Engineering, Louisiana State University, 3508 CEBA Building, Baton Rouge, LA 70803, USA

Received 10 November 1998
CCC 0098–8847/99/121651–17$17·50 *Revised 4 March 1999*
 Accepted 13 July 1999

material or in shape in the horizontal plane. A detailed discussion of the one-dimensional solution for in-plane motion is included in Reference 5.

Since few soil configurations match this homogeneous description, a numerical approach is typically required to capture the influence of any type of irregularity in the surface topography or any inhomogeneity within the soil profile. Numerical analyses have been used by many researchers to study the significance of the soil profile on surface amplification. Early studies investigating surface topography using the boundary element method were made by Bouchon.[6] Other studies examining particular geologic configurations have also been studied. The impact of a canyon in a half-space on wave scattering was treated by Wong[7] using a generalized inverse method. This problem was also solved by Zhao and Valliappan[8] using the finite element method. Inhomogeneities in the soil profile consisting of alluvial deposits have been studied by Bravo and Sanchez-Sesma[9] using Trefftz's method for a two-dimensional alluvial deposit. In a study on seismic response of strip footings supported on alluvial deposits, Dominguez and Abascal[10] determined soil amplification using the boundary element method. In other studies on alluvial deposits, Dravinski studied wave propagation in a single alluvial valley[11] using the source method and by two alluvial valleys in Reference 12. Surface displacements for dipping layers in a half-space due to in-plane body waves were investigated by Eshraghi and Dravinski.[13] In studies considering inclusions, the effect of elastic inclusions in a half-space was studied by Dravinski.[14] A study at an actual site, the Mexico City Valley, was analyzed using a two-dimensional boundary element model by Reinoso *et al.*[15]

Most soil amplification studies have focused on either the surface topography or some type of inhomogeneity within the soil profile. In contrast to the previously mentioned studies, this article investigates a inhomogeneity in the bedrock beneath a soil layer. The soil–bedrock configuration that will be investigated is shown in Figure 1. A horizontal homogeneous viscoelastic soil layer lies on an inhomogeneous rock half-space. The inhomogeneity in the rock half-space is a semi-infinite rock layer comprised of a softer rock material. Table I includes the soil and rock

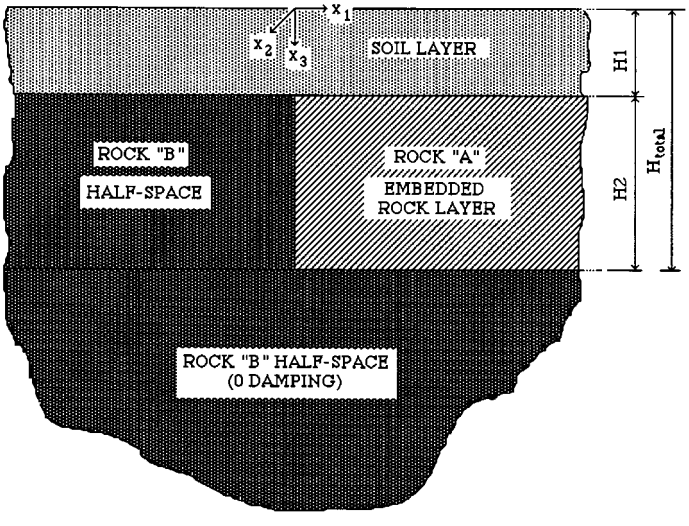

Figure 1. Soil–rock profile

Table I. Soil and rock properties

Soil properties		
Poisson's ratio (v_s)		0·25
Damping (β_s)		5·00%
Rock properties		
	Rock "A"	Rock "B"
Unit wt. ratio (γ_r/γ_s)	1·32	1·32
Poisson's ratio (v_r)	0·25	0·25
Damping β_r	2·00%	1·00%
Shear vel. ratio C_s (rock)/C_s (soil)	Varies	10·00

properties which represent typical values for sand and limestone rock. Hysteretic damping is also included in the study to consider energy loss due to the cyclic loading incurred during seismic activity. In Figure 1, Rock "B" is considered elastic below H_{total} to satisfy requirements for the infinite domain correction discussed later in the article.

To determine the significance of the inhomogeneity in the rock half-space, a parametric study is conducted on the amplification of in-plane body waves as a function of the incident wave type, the half-space incidence angle, embedded rock layer shear velocity, and the embedded rock layer thickness. Three incidence angles are considered: 90, 75, and 60° along with two rock inclusion to soil layer thickness ratios, 1 and 2, and two rock inclusion to soil shear velocity ratios, 2·5 and 5. The results of this study are given as surface displacement plots due to a unit incident wave, P and SV, as a function of dimensionless frequency, $(\omega * H1)/C_{\text{s soil layer}}$. Surface amplifications are calculated for a suite of dimensionless frequencies (0·5, 1·0, 1·2, 1·4, 1·6, 1·8, 2·0, 2·5, and 3·0). For a 20′ thick soil layer with a shear velocity of 1000 fps, these dimensionless frequencies correspond to a frequency range of 4·0–23·9 Hz.

The two-dimensional analysis was made using a boundary element code developed by the author. The boundary integral equations were formulated in the frequency domain using linear elements. The boundary element method was selected for this investigation because of its inherent advantages:

1. the soil–rock configuration can be accurately modelled.
2. the domain problem is simplified to a boundary problem in which only the domain boundaries need to be discretized.
3. the radiation condition is satisfied.

A difficulty that does arise in the method is the modelling of infinite domains. This problem is addressed later in this article.

IN-PLANE BOUNDARY INTEGRAL EQUATION FORMULATION

The derivation of the boundary integral equation in the frequency domain follows. For a more detailed derivation, the reader is suggested to see Reference 16. The in-plane boundary integral equation is derived from Newton's second law using a weighted residual method. The boundary integral equation in the Fourier transformed domain in terms of total and known incident wave

displacement is

$$\bar{u}_k^i(\xi, \omega) = \int_S [\sigma_{mjk}^*(x, \xi, \omega)\bar{u}_m(x, \omega) - u_{mk}^*(x, \xi, \omega)\bar{\sigma}_{mj}(x, \omega)\} n_j(x)\, \mathrm{d}S(x) + \bar{u}_k(\xi, \omega) \tag{1}$$

where the overbar represents the Fourier transform of the variable at the circular frequency ω. In the derivation of equation (1), $+i\omega$ is used for the Fourier transform parameter. The variable $u_k^i(\xi, \omega)$ is the incident wave displacement at ξ along the boundary surface in the k direction at frequency ω. For domains other than a half-space or full-space, $u_k^i(\xi, \omega)$ is equal to 0. $\bar{u}_m(x, \omega)$ is the total displacement at x in the m direction. $\bar{\sigma}_{mj}(x, \omega)$ is the stress at x with m normal in the j direction. The displacement influence function, $u_{mk}^*(x, \xi, \omega)$ and the stress influence function, $\sigma_{mjk}^*(x, \xi, \omega)$, are the displacement and stress, respectively, at x due to a unit force at ξ acting in the k direction.

Equation (1) is rewritten in the Cauchy principle value sense to include for the singularity in the displacement and stress influence functions when x and ξ coincide. Integration of the product of the stress influence function, displacement, and normal near the source point results in a non-zero value which is included in equation (2) as α_{mk}:

$$\bar{u}_k^i(\xi, \omega) = \oint_S [\sigma_{mjk}^*(x, \xi, \omega)\bar{u}_m(x, \omega) - u_{mk}^*(x, \xi, \omega)\bar{\sigma}_{mj}(x, \omega)\} n_j(x)\, \mathrm{d}S(x) + \bar{u}_m(\xi, \omega)[\delta_{mk} + \alpha_{mk}] \tag{2}$$

In the development of the boundary element code, it is easier to work with tractions rather than stress. Therefore, equation (2) is further simplified by replacing the stress terms with tractions:

$$\bar{u}_k^i(\xi, \omega) = \oint_S [\, p_{mk}^*(x, \xi, \omega)\bar{u}_m(x, \omega) - u_{mk}^*(x, \xi, \omega)\bar{p}_m(x, \omega)]\, \mathrm{d}S(x) + \bar{u}_m(\xi, \omega)[\delta_{mk} + \alpha_{mk}] \tag{3}$$

where the traction, $p_m(x)$, is the stress resultant at x in the m direction and is equal to

$$p_m(x) = \sigma_{mj}(x) \cdot n_j(x) \tag{4}$$

Equation (3) is the boundary integral equation used for the development of the boundary element code. The influence functions included in equation (3) are discussed next.

IN-PLANE WAVE INFLUENCE FUNCTIONS

The steady-state displacement influence function for an elastic material is given in Reference 17. In order to include hysteretic damping in the displacement influence function, the correspondence principle is applied to the compression, C_p, and shear, C_s, wave velocities. Assuming that the compression and shear damping are equal to β, the complex wave velocities are

$$C_\mathrm{p}^* = C_\mathrm{p}\sqrt{1 - \mathrm{i}2\beta}, \quad C_\mathrm{s}^* = C_\mathrm{s}\sqrt{1 - \mathrm{i}2\beta} \tag{5}$$

and the corresponding compression and shear wave numbers

$$k_p^* = \omega/C_p^*, \quad k_s^* = \omega/C_s^* \tag{6}$$

The displacement influence function for a material with hysteretic damping is formulated by replacing the real values for the wave numbers in the displacement influence function for an elastic material with their corresponding complex values. The displacement function can then be written as[16]

$$u_{jk}^*(x, \xi, \Omega) = \frac{1}{(\lambda + 2\mu)^*}\left[\delta_{jk} p_1 + p_2 \frac{r_j r_k}{r^2}\right] + \frac{1}{\mu^*}\left[\delta_{jk} s_1 + s_2 \frac{r_j r_k}{r^2}\right] \tag{7}$$

where

$$\begin{aligned} p_1 &= \frac{\mathrm{i}}{8}(H_2^{(1)}(k_p^* r) + H_0^{(1)}(k_p^* r)) - \frac{1}{2\pi(k_p^* r)^2} \\ p_2 &= -\frac{\mathrm{i}}{4} H_2^{(1)}(k_p^* r) - \frac{1}{\pi(k_p^* r)^2} \\ s_1 &= \frac{\mathrm{i}}{8}(H_0^{(1)}(k_s^* r) - H_2^{(1)}(k_s^* r)) + \frac{1}{2\pi(k_s^* r)^2} \\ s_2 &= +\frac{\mathrm{i}}{4} H_2^{(1)}(k_s^* r) - \frac{1}{\pi(k_s^* r)^2} \end{aligned} \tag{8}$$

The displacement influence function in equation (7) is written in terms of the contribution of the compression wave, p, and the shear wave, s, as suggested by Altay.[18]

Substituting the displacement influence function for displacement in Hooke's law results in the stress influence function which in turn can be multiplied by the normal at x to achieve the traction influence function[18]

$$p_{mk}^*(x, \xi, \omega) = n_m \frac{r_k}{r} f_2 + n_k \frac{r_m}{r} f_3 + \delta_{mk} \frac{n_j r_j}{r} f_3 + \frac{n_j r_m r_j r_k}{r^3} f_1 \tag{9}$$

where

$$\begin{aligned} f_1 &= \frac{\mathrm{i}}{r}\left\{\left[\frac{k_p^*}{k_s^*}\right]^2\left[2H_2^{(1)}(k_p^* r) - \frac{k_p^* r}{2} H_1^{(1)}(k_p^* r)\right] - 2H_2^{(1)}(k_s^* r) + \frac{k_s^* r}{2} H_1^{(1)}(k_s^* r)\right\} \\ f_2 &= \frac{\mathrm{i}}{r}\left\{\left(1 - 2\left[\frac{k_p^*}{k_s^*}\right]^2\right)\left[-\frac{k_p^* r}{4} H_1^{(1)}(k_p^* r)\right] - \frac{1}{2}\left[\frac{k_p^*}{k_s^*}\right]^2 H_2^{(1)}(k_p^* r) + \frac{1}{2} H_2^{(1)}(k_s^* r)\right\} \\ f_3 &= \frac{\mathrm{i}}{4r}\left\{\left(-2\left[\frac{k_p^*}{k_s^*}\right]^2\right) H_2^{(1)}(k_p^* r) + 2H_2^{(1)}(k_s^* r) - (k_s^* r) H_1^{(1)}(k_s^* r)\right\} \end{aligned} \tag{10}$$

DOMAIN TRUNCATION CORRECTION FOR IN-PLANE WAVES

A problem that arises in the use of the boundary element method for infinite domain regions is how to correctly discretize an open domain. Typically infinite domains are discretized to a

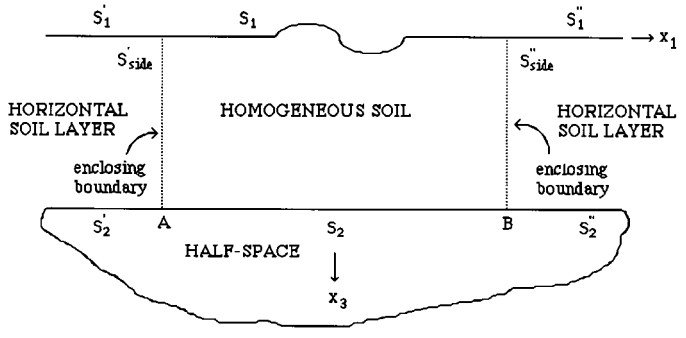

Figure 2. Correction for domain truncation

limit outside of which is considered to have negligible effect on the interested study area. For regions of low damping, this limit may be fairly large. A method is suggested for layer discretization which is similar to the approach proposed by Hadley *et al.* for elastic anti-plane shear waves.[19] Here the method is extended and applied to in-plane body waves in a viscoelastic material.

Figure 2 shows a soil layer on a rock half-space. The soil layer includes some type of an irregularity at the surface. Discretization along the top and bottom boundaries are discretized to a distance far enough from the irregularity so that scattering due to the surface irregularity is negligible. Therefore, at this limit point displacements and tractions can be taken as the values from a one-dimensional analysis. To correct for the truncated portion of the soil layer, fictitious enclosing boundaries are drawn to create a closed domain. Therefore, the open domain is transferred to an enclosed domain. Along the enclosing boundaries, the displacements and tractions are taken equal to the one-dimensional analysis solution. Rectifying the truncation problem in the half-space domain is more complicated. One method, suggested by Ahmad and Banerjee,[20] uses enclosing elements for the half-space. Here an alternative approach is suggested. In this formulation, the half-space domain is assumed to be elastic and its boundary horizontal (Figure 2). Outside of the enclosing boundary of the soil layer, the free-field displacements and tractions are taken as the solution of the one-dimensional analysis. Therefore, along the horizontal boundary of the half-space outside of the enclosing boundaries the displacements and tractions are a function of $\exp(ikx_1)$. In order to simplify the correction for the half-space boundary truncation, and since rock damping is typically small, an elastic material is assumed for the half-space.

For a half-space boundary, the part of the boundary integral equation (3), which includes traction is

$$\int_{+\infty}^{-\infty} [u_{ik}^{*}(x, \xi, \omega)\, \mu_{\mathrm{hs}}] \left[\frac{\bar{p}_i(x, \omega) H1}{\mu_{\mathrm{hs}}} \right] \mathrm{d}(x_1/H1) \tag{11}$$

where μ_{hs} is the half-space shear modulus. Accordingly, the entire boundary of the half-space should be discretized. In lieu of this requirement the equation is rewritten so as to have a lower bound limit of B and an upper bound limit of A with a correction for the truncated

portion of the boundary, Figure 2. Therefore, the required correction for truncation of the traction integral is

$$\int_{+\infty}^{B} [u_{ik}^{*}(x, \xi, \omega)\,\mu_{\mathrm{hs}}] \left[\frac{\bar{p}_i(x, \omega)H1}{\mu_{\mathrm{hs}}}\right] \mathrm{d}(x_1/H1) + \int_{A}^{-\infty} [u_{ik}^{*}(x, \xi, \omega)\,\mu_{\mathrm{hs}}] \left[\frac{\bar{p}_i(x, \omega)H1}{\mu_{\mathrm{hs}}}\right] \mathrm{d}(x_1/H1) \tag{12}$$

Similarly, for the displacement boundary integral, the required correction for the truncated portion is

$$\int_{+\infty}^{B} [\,p_{ik}^{*}(x, \xi, \omega)H1]\,\bar{u}_i(x)\,\mathrm{d}(x_1/H1) + \int_{A}^{-\infty} [\,p_{ik}^{*}(x, \xi, \omega)H1]\,\bar{u}_i(x)\,\mathrm{d}(x_1/H1) \tag{13}$$

The methodology of solving for the solutions for equations (12) and (13) can be found in an earlier manuscript by Heymsfield.[21] In previous studies by the author, including these corrections for truncation have been found to be important in order that the numerical results compare favourably with analytic solutions.

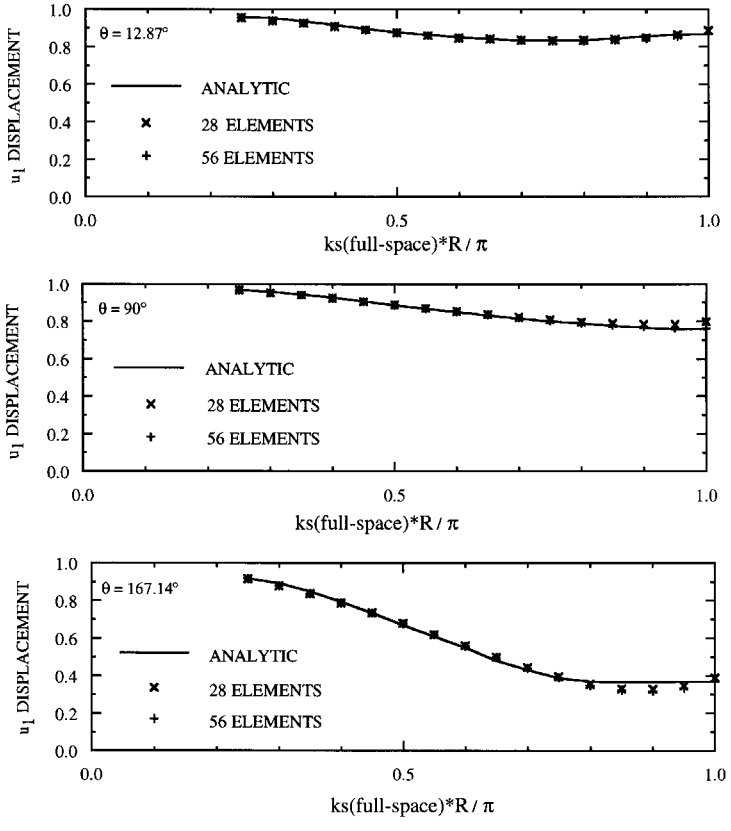

Figure 3. Elastic inclusion in a full space, u_1 displacement due to an incident P wave

CODE VALIDATION

The boundary element code used in this analysis for a rock discontinuity was developed by the author. The code is validated in this section by comparing results of the code with analytic solutions. Since the number of cases that an analytic solution exists is limited, problems which have been solved by others using numerical techniques were also used for validation.

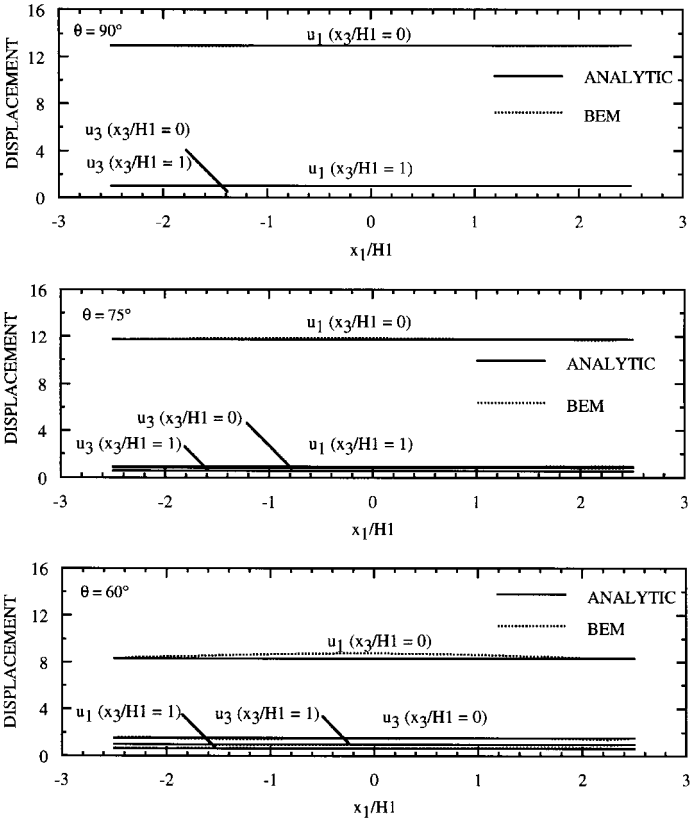

Figure 4. Single layer on an elastic half-space, displacement due to an incident SV wave with $ks_1 * H1 = 1{\cdot}5708$

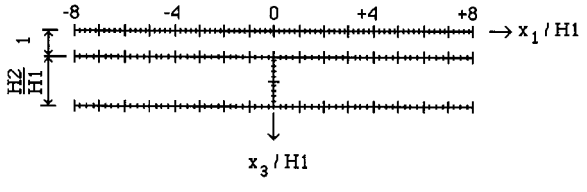

Figure 5. Boundary element discretization

One problem in which an analytic solution exists is an elastic cylindrical inclusion in an elastic full-space. The exact solution for the problem is developed using a series solution as discussed in Pao and Mow [22] where the solution is given in terms of displacement potentials. The results of the problem in terms of displacement for a cylindrical inclusion with a shear modulus twice that of the full-space is given in Reference 10. Both of the materials in the problem have equal unit weights and a Poisson's ratio of 0·25. Solution for the problem is given at specific points along the circumference of the inclusion as displacements parallel to the direction of the incident wave, u_1. A comparison between the analytic solution and the code solution is given in Figure 3 where θ is measured off the incident wave direction and locates a point along the circumference of the inclusion.

For the boundary element code validation, two boundary element schemes are tried, one with 28 linear elements of equal length, $\Delta\theta = 12{\cdot}86^\circ$, and a second case with 56 linear elements, $\Delta\theta = 6{\cdot}43^\circ$. Only small variation is found between these two discretization cases. Comparison of the boundary element solution with the analytic solution shows good agreement. However, discrepancy occurs at the higher frequencies along the scattering face of the inclusion, $\theta = 167{\cdot}14^\circ$. Since linear elements are used in the code, in order to develop a more

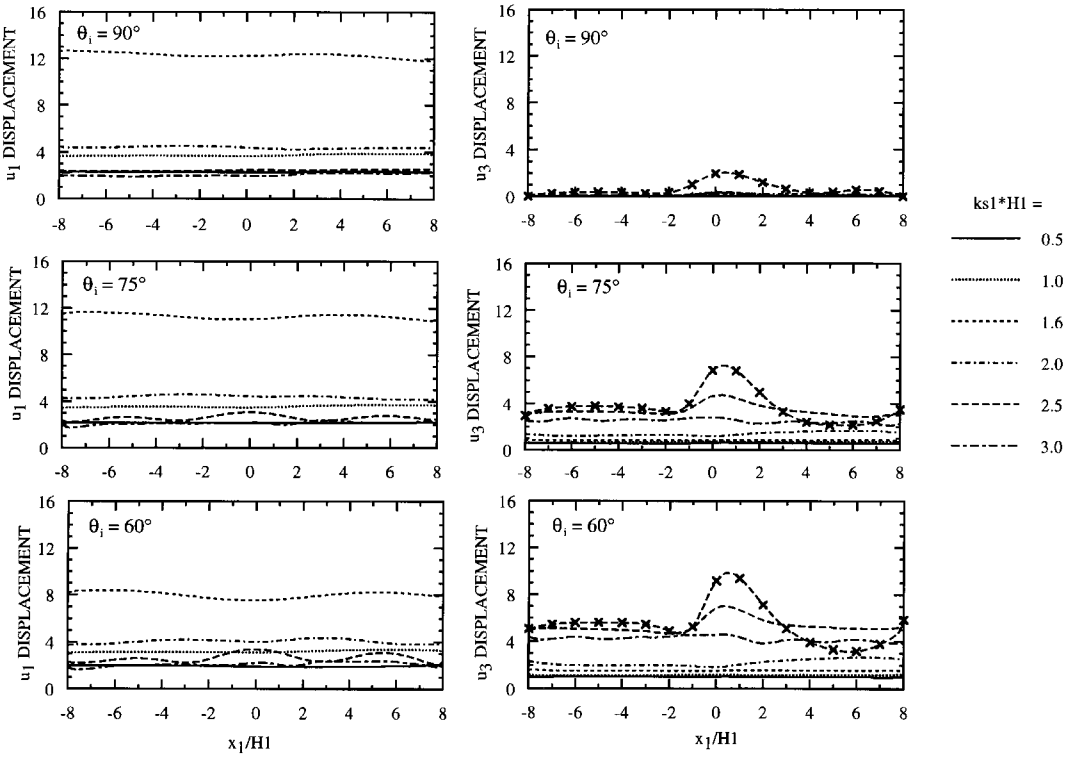

Figure 6. Surface displacement due to a unit incident SV wave, C_s rock "A"/C_s soil = 5, $H2/H1 = 1{\cdot}0$ (X; $ks1 * H1 = 2{\cdot}5$ & $H2/H1 = 2{\cdot}0$)

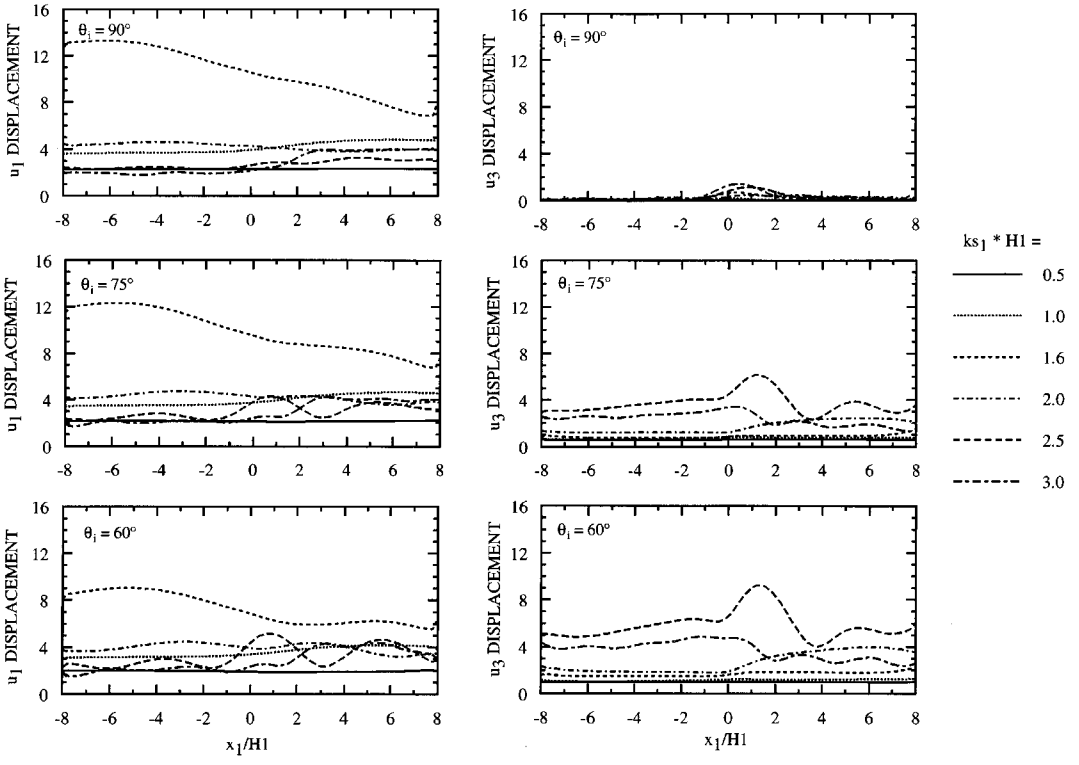

Figure 7. Surface displacement due to a unit incident SV wave, C_s rock "A"/C_s soil = 2·5, $H2/H1 = 1{\cdot}0$

accurate solution for this problem, more elements are required to model the curvature of the inclusion face.

A second problem with an analytic solution is a horizontal homogeneous soil layer on a rock half-space. The analytic solution can be found from a one-dimensional analysis. A homogeneous soil layer with 5·0 per cent damping rests on an elastic rock half-space which is subjected to in-plane SV body waves. The shear velocity ratio and unit weight ratio of the half-space to soil layer are 10 and 1·32, respectively. In the numerical analysis, the horizontal boundaries of the soil layer and the half-space are discretized to $\pm$ 2·5 times the soil layer thickness, $H1$, at $0{\cdot}25 * H1$ intervals.

Figure 4 shows the displacement amplifications along the boundaries due to a unit incident SV wave. Displacements are shown for a dimensionless frequency of 1·5708 and for a suite of incidence angles: 90, 75, and 60°. The frequency used corresponds to the natural frequency for a soil layer subjected to vertically propagating shear waves. The figure shows good agreement with the analytic solution. A small error develops when the angle of incidence equals 60° for the incident SV wave due to the increased coupling which occurs between the horizontal and vertical motions. The solutions near the limits of discretization coincide with the analytic solution indicating the sufficiency of the correction for truncation included in the code.

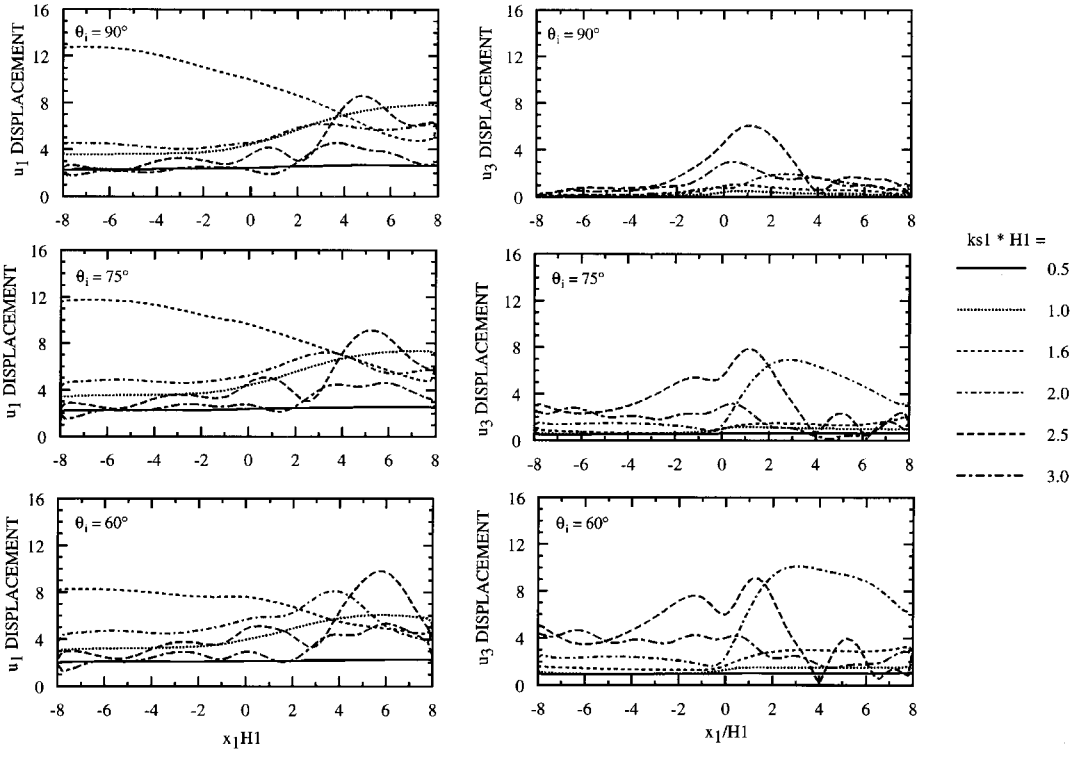

Figure 8. Surface displacement due to a unit incident SV wave, C_s rock "A"/C_s soil = 2·5, $H2/H1 = 2{\cdot}0$

TWO-DIMENSIONAL ANALYSIS

In order to solve for the surface displacement for the soil–bedrock configuration shown in Figure 1, a two-dimensional study is executed using the boundary element method. The boundary discretization scheme used for the analysis is shown in Figure 5. Along the surface, the boundary is segmented using $0{\cdot}2 * H1$ lengths. This segment length is also used along the vertical boundary at $x_1 = 0$. This length corresponds to one-tenth of the minimum wave length used in the study. Along the other horizontal boundaries, the element lengths are taken as $0{\cdot}25 * H1$ which corresponds to one-eighth of the minimum wave length. These segment lengths were chosen to try to capture the high surface amplification along the surface boundary and the high expected variability along the vertical discontinuity face. In the vicinity where the three domains meet, a shorter element length was used to include for high fluctuation in this region.

Surface displacements for a unit in-plane wave are calculated for a range of dimensionless frequencies, $ks1 * H1$, equal to: 0·5, 1·0, 1·2, 1·4, 1·6, 1·8, 2·0, 2·5, and 3·0 as a function of the embedded rock layer thickness and shear velocity ratio. At each frequency, surface displacements are calculated at incidence angles of 90, 75, and 60°. Results of the two-dimensional

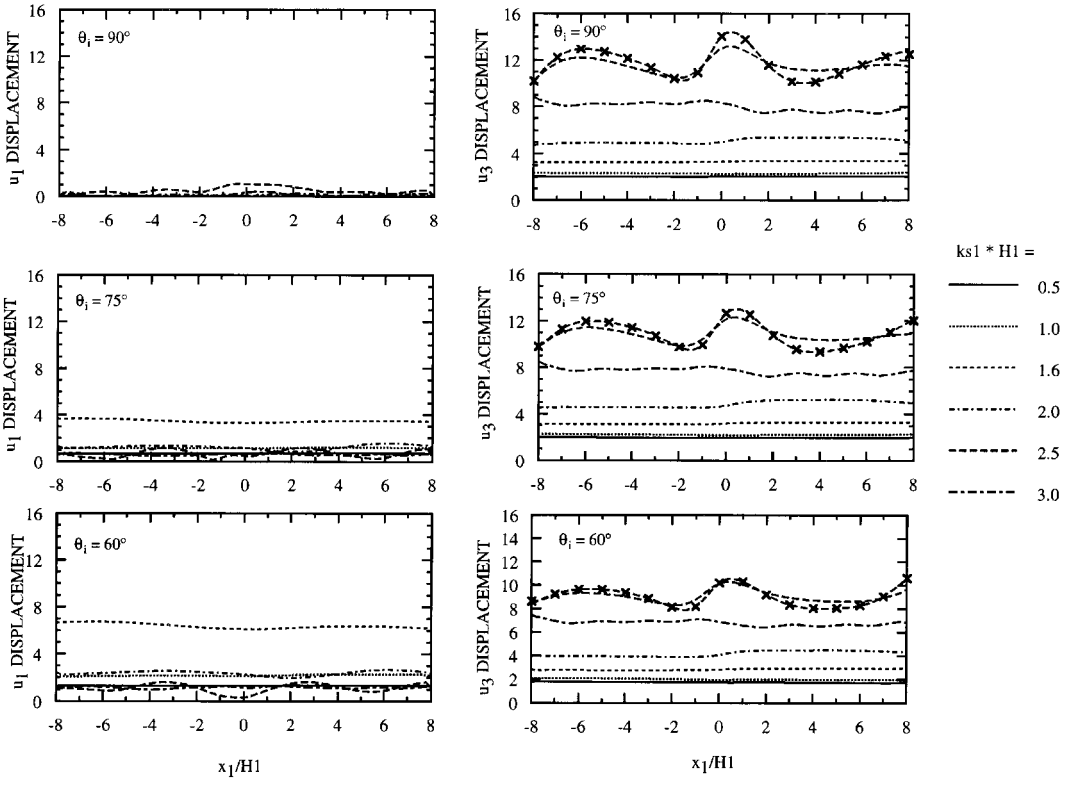

Figure 9. Surface displacement due to a unit incident P wave, C_s rock "A"/C_s soil = 5, $H2/H1 = 1{\cdot}0$ (X; $ks1 * H1 = 2{\cdot}5$ & $H2/H1 = 2{\cdot}0$)

study are given in Figures 6–8 for an incident SV wave and in Figures 9–11 for an incident P wave. In these figures, amplification functions are shown only at $ks1 * H1 = 0{\cdot}5$, 1·0, 1·6, 2·0, 2·5, and 3·0 for reasons of clarity. In order to incorporate the correction for truncation mentioned previously, displacements at $x_1/H1 = \pm 8$ are assumed equal to the one-dimensional analysis solution. Summaries of natural frequencies and corresponding surface amplitudes from the one-dimensional analysis solution are given in Tables II and III for incident SV and P waves, respectively.

SURFACE DISPLACEMENTS DUE TO A UNIT INCIDENT SV WAVE

An incident SV wave in the rock half-space generates both horizontal and vertical surface displacement. Surface displacements, horizontal and vertical, as a function of frequency and location along the horizontal surface boundary are given in Figures 6–8. In Figure 6, the shear velocity ratio of the embedded rock layer is equal to 5 and the embedded rock layer thickness is the same as the soil layer. Superimposed on Figure 6 are the vertical displacements at

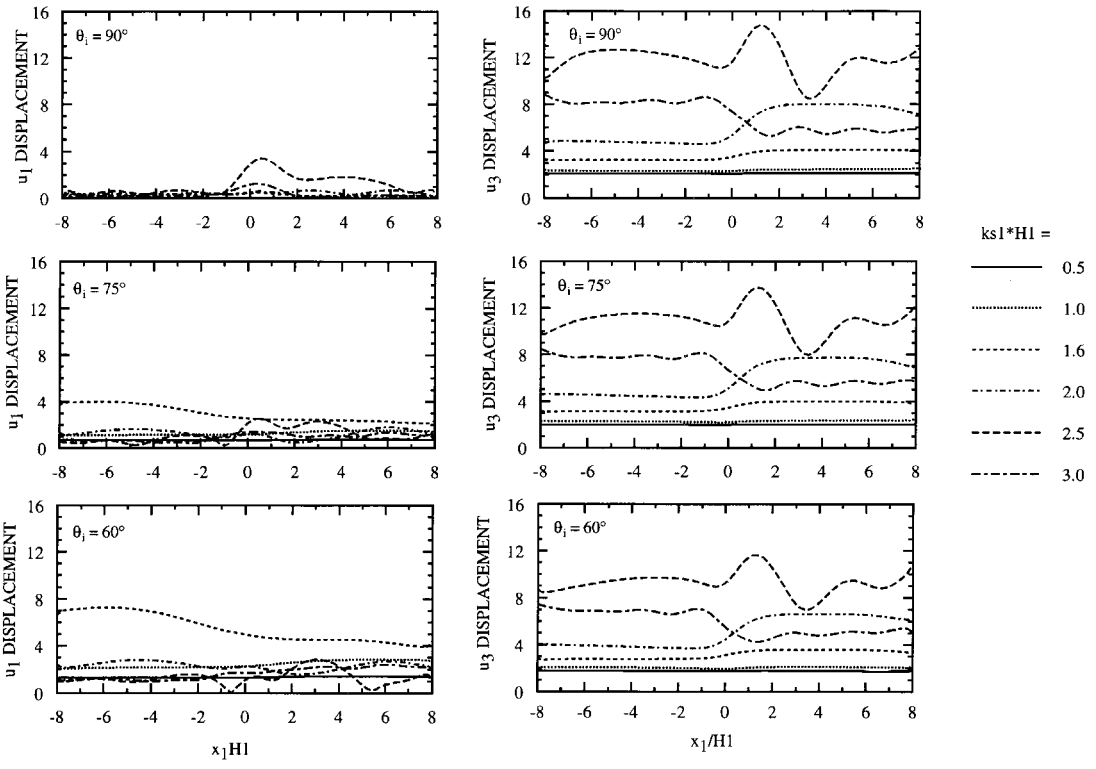

Figure 10. Surface displacement due to a unit incident P wave, C_s rock "A"/C_s soil = 2·5, $H2/H1 = 1{\cdot}0$

a dimensionless frequency of 2·5 when the embedded layer is doubled. Figures 7 and 8 consider a softer embedded rock layer in which the shear velocity ratio is 2·5. In Figure 7 the rock layer thickness is the same as the soil layer while in Figure 8 the rock layer thickness is twice that of the soil layer.

Surface displacements are shown in Figure 6 for the case of the embedded rock layer thickness and soil layer thickness equal to each other. For frequencies less than 2, horizontal displacements show smooth transition along the boundary surface. However, for frequencies above 2, increased scattering due to the discontinuity results in greater fluctuation. In contrast to the one-dimensional analysis, vertical displacement exists for a vertically incident SV wave. For frequencies other than 2·5, vertical displacement varies fairly smoothly. At $ks1 * H1 = 2{\cdot}5$, vertical displacement is magnified above the embedded rock layer near the discontinuity which is not anticipated from the one-dimensional analysis. Within the considered frequency range, maximum vertical displacement occurs in the proximity of the rock discontinuity at the frequency closest to the vertical displacement fundamental frequency of the one-dimensional solution. In Figure 6, horizontal displacements decrease as the half-space incidence angle decreases while vertical displacement increases. Similar results to this case are found when the embedded rock layer is doubled. Within the frequency range, only for a frequency of 2·5 does the vertical displacement for

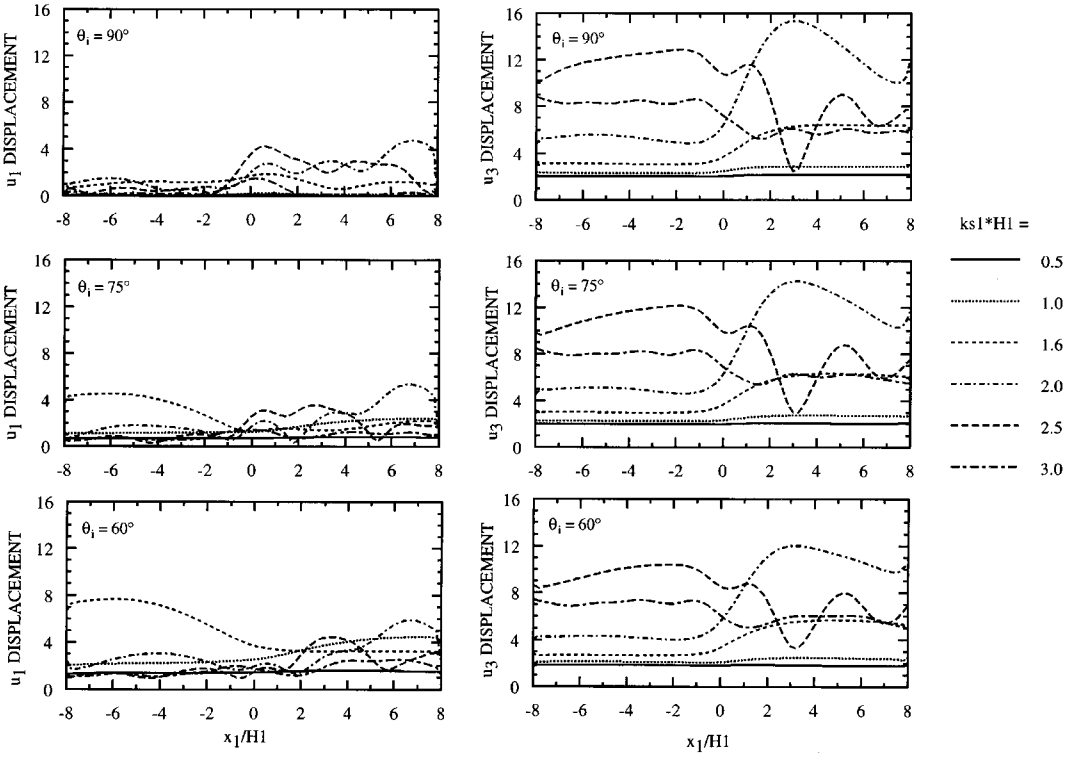

Figure 11. Surface displacement due to a unit incident P wave, C_s rock "A"/C_s soil = 2·5, $H2/H1 = 2{\cdot}0$

the $H2/H1 = 2$ case significantly differ from the $H2/H1 = 1$ case. The results for this particular case which show greater amplification in the vicinity of the rock discontinuity are superimposed on Figure 6.

A reduction in the shear stiffness of the embedded rock layer, Figures 7 and 8, results in increased scattering in the higher frequencies, 2·5 and 3·0. Fluctuation of the horizontal displacement occurs above the embedded rock layer. Amplified vertical displacements due to scattering occur over the embedded rock layer and appear to be limited to a region near the vertical discontinuity. Increasing the embedded rock layer thickness for this case, Figure 8, significantly increases scattering for frequencies of 2·0 and above. Accompanying this greater thickness, the vertical motion fluctuation in the vicinity of the vertical discontinuity encompasses a larger region on both sides of $x_1 = 0$.

SURFACE DISPLACEMENTS DUE TO A UNIT INCIDENT P WAVE

Figures 9–11 examine the surface response behaviour due to an incident P wave. Figure 9 includes plots of the surface response if the stiffness of the embedded rock layer is half that of the

Table II. Natural frequencies and corresponding amplitudes due to an incident SV wave using a one-dimensional analysis solution

Horizontal displacement

$H2/H1$	C_s2/C_s1	First natural frequency $n = 1$ (fundamental frequency)				Second natural frequency $n = 2$			
		$ks1 * H1$	θ incident			$ks1 * H1$	θ incident		
			90·0	75·0	60·0		90·0	75·0	60·0
1·0	10·0	1·6	13·0	11·8	8·3	4·7	6·4	5·9	4·8
	5·0	1·5	13·1	11·9	8·3	4·6	7·2	6·6	5·0
	2·5	1·4	13·6	12·2	8·3	3·7	6·4	5·8	3·94
2·0	10·0	1·6	13·0	11·8	8·3	4·7	6·4	5·9	4·8
	5·0	1·5	13·1	11·8	8·3	4·8	7·0	6·6	5·6
	2·5	1·2	12·6	11·3	7·4	2·3	7·7	7·0	4·9

Vertical displacement

$H2/H1$	C_s2/C_s1	First natural frequency $n = 1$ (fundamental frequency)				Second natural frequency $n = 2$			
		$ks1 * H1$	θ incident			$ks1 * H1$	θ incident		
			90·0	75·0	60·0		90·0	75·0	60·0
1·0	10·0	2·7	0·0	3·7	6·4	> 5			
	5·0	2·7	0·0	3·8	6·4	> 5			
	2·5	2·4	0·0	3·9	6·5	> 5			
2·0	10·0	2·7	0·0	3·7	6·4	> 5			
	5·0	2·6	0·0	3·6	6·1	> 5			
	2·5	2·0	0·0	3·3	5·6	3·9	0·0	2·0	3·2

half-space. When the rock layer has a thickness equal to the soil layer, except for a frequency equal to 2·5, surface displacement varies smoothly from the one dimensional solution at the enclosing boundary point on either side of the discontinuity. At all incidence angles, horizontal displacements are generated. At $ks1 * H1 = 2{\cdot}5$, a peak occurs in the vertical displacement above the embedded rock layer in the vicinity of the discontinuity. Increasing $H2$ at this frequency results in increased scattering while for the other frequencies there is little difference between the two thicknesses. Superimposed on Figure 9 are the vertical displacements considering doubling the embedded rock layer. Decreasing the shear velocity of the embedded rock layer, Figures 10 and 11, increases the fluctuation of the horizontal motion above the rock layer. For the lower frequencies, 0·5–2·0, motion varies fairly smoothly within a transition zone between the one-dimensional solutions on either side of the discontinuity. Figure 11, $H2/H1 = 2$, shows the broader region in which vertical displacement is amplified due to the scattering which the discontinuity causes.

Table III. Natural frequencies and corresponding amplitudes due to an incident P wave using a one-dimensional analysis solution

Horizontal displacement

$H2/H1$	C_s2/C_s1	First natural frequency $n = 1$ (fundamental frequency)				Second natural frequency $n = 2$			
		$ks1 * H1$	θ incident			$ks1 * H1$	θ incident		
			90·0	75·0	60·0		90·0	75·0	60·0
1·0	10·0	1·6	0·0	3·8	6·8	4·7	0·0	1·8	3·4
	5·0	1·5	0·0	3·8	6·8	4·6	0·0	2·0	3·6
	2·5	1·4	0·0	3·9	7·0	3·6	0·0	1·7	3·0
2·0	10·0	1·6	0·0	3·8	6·8	4·7	0·0	1·8	3·4
	5·0	1·5	0·0	3·8	6·8	4·7	0·0	1·5	2·7
	2·5	1·2	0·0	3·6	6·4	2·4	0·0	1·9	3·3

Vertical displacement

$H2/H1$	C_s2/C_s1	First natural frequency $n = 1$ (fundamental frequency)				Second natural frequency $n = 2$			
		$ks1 * H1$	θ incident			$ks1 * H1$	θ incident		
			90·0	75·0	60·0		90·0	75·0	60·0
1·0	10·0	2·7	13·0	12·4	10·9	> 5			
	5·0	2·7	13·1	12·6	11·1	> 5			
	2·5	2·4	13·6	13·0	11·5	> 5			
2·0	10·0	2·7	13·0	12·4	10·9	> 5			
	5·0	2·6	13·1	12·6	11·1	> 5			
	2·5	2·1	12·6	12·1	10·8	4·0	7·7	7·4	6·5

CONCLUSIONS

A two-dimensional analysis has been performed to investigate the seismic behaviour for a soil–rock configuration in which a discontinuity in the half-space exists. Results are determined as a function of dimensionless parameters for in-plane body waves. Surface displacements indicate that at the lower dimensionless frequencies, below 2·0, smooth transition occurs between the one-dimensional solution on either side of the discontinuity. Higher frequencies, 2·0, 2·5, and 3·0, cause increased scattering accompanied with high vertical displacements which are greater than that expected from the one-dimensional solution. Although the one-dimensional solution is adequate at low frequencies, the surface behaviour at the higher frequencies indicates the need for a two-dimensional solution to determine regions of fluctuation and increased displacement.

REFERENCES

1. E. Heymsfield, 'Two-Dimensional Scattering of SH Waves due to a discontinuity in bedrock', *Earthquake Engng. Struct. Dyn.* **28**(8), 841–855 (1999).
2. F. J. Sanchez-Sesma, 'Site effects on strong ground motion', *Soil Dyn. Earthquake Engng.* **6**, 124–132 (1987).
3. J. A. Rial, N. G. Saltzman and H. Ling, 'Earthquake-induced resonance in sedimentary basins', *Amer. Scientist* **80**, 566–578 (1992).
4. W. D. Finn, C. E. Ventura and N. D. Schuster, 'Ground motions during the 1994 northridge earthquake', *Can. J. Civil Engng.* **22**, 300–315 (1995).
5. J. P. Wolf, *Dynamic Soil–Structure Interaction*, Prentice-Hall, NJ, 1985.
6. M. Bouchon, 'Effect of topography on surface motion', *Bull. Seismol. Soc. Amer.* **63**, 615–632 (1973).
7. H. L. Wong, 'Effect of surface topography on the diffraction of P, SV, and Rayleigh waves', *Bull. Seismol. Soc. Amer.* **72**, 1167–1183 (1982).
8. C. Zhao and S. Valliapan, 'Incident P and SV wave scattering effects under different canyon topographic and geological conditions', *Int. J. Numer. Anal. Methods Geomech.* **17**, 73–94 (1993).
9. M. A. Bravo and F. J. Sanchez-Sesma, 'Seismic response of alluvial valleys for incident P, SV, and Rayleigh waves', *Soil Dyn. Earthquake Engng.* **9**, 16–19 (1990).
10. J. Dominguez and R. Abascal, 'Seismic response of strip footings on zoned viscoelastic soils', *J. Engng. Mech.* **115**, 913–934 (1989).
11. M. Dravinski, 'Scattering of elastic waves by an alluvial valley', *J. Engng. Mech. Div. ASCE* **108**, 19–31 (1982).
12. M. Dravinski, 'Amplification of P, SV, and Rayleigh waves by two alluvial valleys', *Soil Dyn. Earthquake Engng.* **2**, 66–77 (1983).
13. H. Eshraghi and M. Dravinski, 'Transient scattering of elastic waves by dipping layers of arbitrary shape. Part 2: Plane strain model', *Earthquake Engng. Struct. Dyn.* **18**, 417–434 (1989).
14. M. Dravinski, 'Ground motion amplification due to elastic inclusions in a half-space', *Earthquake Engng. Struct. Dyn.* **11**, 313–335 (1983).
15. E. Reinoso, L. C. Wrobel and H. Power, 'Two-dimensional scattering of P, SV and Rayleigh waves: preliminary results for the valley of Mexico', *Earthquake Engng. Struct. Dyn.* **26**, 595–616 (1997).
16. E. Heymsfield, 'Application of the boundary integral equation method to a discontinuity in bedrock', Ph.D. Thesis, City University of New York, 1995.
17. P. K. Banerjee and R. Butterfield, *Boundary Element Methods in Engineering Science*, McGraw-Hill, London, 1981.
18. S. Altay, 'Explicit integration of boundary integral equations in the frequency domain for wave scattering', Ph.D. Thesis, Princeton University, 1986.
19. P. K. Hadley, A. Askar and A. S. Cakmak, 'Scattering of waves by inclusions in a nonhomogeneous elastic half space solved by boundary element methods', NCEER-89-0027, National Center For Earthquake Engineering Research, 1989.
20. S. Ahmad and P. K. Banerjee, 'Multi-domain BEM for two-dimensional problems of elastodynamics', *Int. J. Numer. Methods Engng.* **26**, 891–911 (1988).
21. E. Heymsfield, 'Infinite Domain Correction For In-Plane Body Waves in a Two-Dimensional Boundary Element Analysis', *Int. J. Numer. Methods Engng.* **40**, 1687–1700 (1997).
22. Y. Pao and C. Mow, *Diffraction of Elastic Waves and Dynamic Stress Concentrations*, Crane, Russak and Company Inc., New York, 1973.

